cells

MDPI

Article

MicroRNA-101 Perturbation Is Associated with Myogenic and Intramyocellular Lipid Phenotypes in Fetal Bovine Muscle Satellite Cells

Elke Albrecht [1], Asghar Ali [1,2], Kristoffer Ström [3], Suraya Sabreen [4], Majid Ali [5], Mamatha Philip Gabriel [6], Ola Hansson [3,7], Steffen Maak [1,*] and Bilal Ahmad Mir [1,3,*]

1 Research Institute for Farm Animal Biology, 18196 Dummerstorf, Germany; elke.albrecht@fbn-dummerstorf.de (E.A.); ali@genzentrum.lmu.de (A.A.)
2 Chair for Molecular Animal Breeding and Biotechnology, Gene Centre, Ludwig Maximilian University of Munich (LMU), 81377 Munich, Germany
3 Department of Clinical Sciences, Lund University Diabetes Centre, Lund University, 20502 Malmö, Sweden; kristoffer.strom@med.lu.se (K.S.); ola.hansson@med.lu.se (O.H.)
4 Department of Mechanical Engineering, Sejong University, Seoul 05006, Republic of Korea
5 Department of Life Sciences, School of Natural Sciences, Shiv Nadar Institution of Eminence, Greater Noida 201314, India
6 First Year College and Institute of Health and Sport, Victoria University, Melbourne, VIC 8001, Australia; mamatha.philipgabriel@vu.edu.au
7 Institute for Molecular Medicine Finland (FIMM), Helsinki University, 00290 Helsinki, Finland
* Correspondence: maak@fbn-dummerstorf.de (S.M.); bilal.mir@med.lu.se (B.A.M.)

Abstract

MicroRNAs (miRNAs) are important post-transcriptional regulators of skeletal muscle development and metabolism. In our previously published expression profiling of bovine longissimus dorsi muscle with divergent intramuscular fat (IMF) content, miR-101 was more abundant in high-IMF muscle whereas *PROX1* showed an inverse expression pattern, motivating the present study. We examined the consequences of miR-101 gain- and loss-of-function in primary fetal bovine muscle satellite cells (BMSCs) and, as a supporting sequence-level experiment, tested a predicted miR-101 seed-matching site in the bovine *PROX1* 3′ untranslated region (3′UTR) using a heterologous C2C12 reporter system. During BMSC differentiation, miR-101 decreased initially and subsequently increased, whereas *PROX1* expression showed the opposite temporal pattern. AgomiR increased miR-101 abundance approximately 870-fold and antagomiR reduced it by approximately 85%, confirming effective manipulation. However, neither treatment significantly altered endogenous *PROX1* mRNA abundance or the PROX1-immunoreactive signal. The manipulation of miR-101 produced selective, non-uniform changes in myogenic markers and did not significantly affect BrdU incorporation. Unexpectedly, both miR-101 overexpression and inhibition increased oleic-acid-induced lipid-particle number and lipid-covered area while reducing interparticle distance; however, mean particle size was significantly lower with agomiR than antagomiR. AgomiR also reduced *CD36* and *FABP4* transcripts, with additional trends for *ACADM* and *FABP3*. In the C2C12 reporter assay, miR-101 reduced activity of the wild-type *PROX1* 3′UTR reporter, whereas disruption of the *PROX1* seed-matching site abolished repression. Overall, during myogenic differentiation of BMSC, miR-101 perturbation altered the expression of selected genes involved in myogenic differentiation and lipid handling, whereas endogenous *PROX1* mRNA abundance and the *PROX1*-immunoreactive signal were not significantly affected.

Check for updates

Academic Editor: Gillian Sandra Butler-Browne

Received: 23 October 2026
Revised: 25 November 2026
Accepted: 25 November 2026
Published: 27 November 2026

Copyright: © 2026 by the authors. Licensee MDPI, Basel, Switzerland. This article is an open access article distributed under the terms and conditions of the Creative Commons Attribution (CC BY) license.

Keywords: miR-101; PROX1; bovine muscle satellite cells; myogenesis; muscle fiber type; intramyocellular lipid; microRNA; fatty-acid metabolism

1. Introduction

Skeletal muscle development is a highly coordinated process involving the activation, proliferation and differentiation of muscle progenitor cells [1]. Satellite cells constitute the principal myogenic precursor population responsible for postnatal muscle mass and regeneration [1,2]. Beyond its contractile function, skeletal muscle is a major metabolic tissue in which fiber-type composition, mitochondrial capacity and intracellular lipid content influence substrate utilization and physiological performance and, in livestock, contribute to economically important carcass and meat-quality traits [2–5]. Intramuscular fat (IMF) is a complex phenotype comprising lipid stored in intramuscular adipocytes as well as neutral lipid accumulated within muscle fibers [6,7]. In vitro, exposure of differentiated muscle cells to free fatty acids such as oleic acid promotes intracellular triglyceride accumulation, as demonstrated in bovine, C2C12 and human myotubes [8–10]. The progression of proliferating myoblasts into differentiated multinucleated myotubes, together with muscle fiber-type specification and lipid deposition, is tightly regulated by myogenic and non-myogenic transcription factors and signaling pathways.

Prospero-related homeobox 1 (*PROX1*) is a transcription factor with an established role in skeletal muscle development and fiber-type specification [11,12]. In rodent and human skeletal muscle, PROX1 is expressed in satellite cells and is enriched in slow muscle fibers. Gain- and loss-of-function studies have shown that PROX1 promotes the slow-fiber transcriptional program, including expression of *MYH7*, whereas loss of PROX1 induces a shift toward the fast twitch fiber phenotype [11,12]. Consistent with these findings, the relevance of *PROX1* to livestock porcine muscle is supported in a study where *PROX1* expression is higher in oxidative soleus than in biceps femoris muscle, parallels expression of MyHC I and myoglobin, and is associated with meat redness, drip loss and muscle fiber composition [13]. Given its essential role in myogenic differentiation and fiber identity, understanding the mechanisms that regulate *PROX1* expression, including post-transcriptional regulation, is important for elucidating how skeletal muscle phenotype is established and maintained.

MicroRNAs (miRNAs) are short non-coding RNAs that post-transcriptionally regulate gene expression, most commonly through sequence-dependent interactions with the 3′ untranslated region (3′UTR) of target transcripts, thereby coordinating multiple developmental and metabolic pathways [14–18]. Previously published studies on miR-101 suggest a stage- and context-dependent role in myogenesis [19,20]. In Qinchuan cattle, miR-101-1 was detected across skeletal-muscle developmental stages, with the highest abundance in calf, followed by adult and fetal muscle [19]. The authors also reported increased expression during myogenic differentiation and altered C2C12 myotube formation after experimental overexpression [19]. More recently, miR-101a/b was shown to undergo transient induction during C2C12 differentiation and to restrain myogenic differentiation by directly targeting MEF2A and modulating p38/MAPK, Wnt and other myogenic signaling pathways [20]. *PROX1* is also subject to miRNA-mediated regulation in non-muscle systems, miR-181a and miR-31 repress *PROX1* during lymphatic endothelial specification [21,22], while miR-466, miR-205 and miR-489 have been reported to target the *PROX1* 3′UTR in lymphatic endothelial or cancer cells [23–25]. In our previously published profiling of bovine longissimus dorsi muscle with divergent IMF content, miR-101 was more abundant in high-IMF muscle whereas *PROX1* showed an inverse expression pattern [26,27]. Based on this association, the present study primarily examined how miR-101 gain- and loss-of-function affect en-

dogenous *PROX1*, myogenic and fiber-type-associated markers, as well as cell proliferation and oleic-acid-induced intramyocellular lipid accumulation in primary BMSC. In parallel, a heterologous C2C12 luciferase assay was used as a complementary test of whether the predicted bovine *PROX1* 3′UTR seed-matching site is responsive to miR-101.

2. Materials and Methods

2.1. Prediction of the PROX1 miR-101 Seed-Matching Site and Heterologous Dual-Luciferase Reporter Assay

Predicted miR-101 target sites were assessed using TargetScan 7.2 (http://www.targetscan.org/vert_72/ (accessed on 20 November 2021)), and conservation of the candidate region across vertebrate *PROX1* 3′UTRs was examined [28]. Here, the term miR-101 seed refers to the seed region of the miRNA, whereas seed-matching site refers to the complementary sequence in *PROX1* 3′UTR. A conserved seed-matching site was identified at positions 5077–5084 of the bovine *PROX1* 3′UTR. The reporter workflow followed our previously published study [10]. Briefly, the wild-type *PROX1* target region was cloned into the pmirGLO dual-luciferase reporter vector. The wild-type oligonucleotide contained the predicted miR-101 seed-matching sequence 5′-GTACTGTA-3′. In the mutant cloning oligonucleotide, this region was replaced by the poly-T segment shown below, disrupting complementarity with the miR-101 seed region. The relevant wild-type and mutant sense and antisense oligonucleotides were:

- WT sense: 5′-pAAACTAGCGGCCGCATTACCAAGGAT**GTACTGTA**ATATTAATTGATTCTAG-3′;
- WT antisense: 3′-pTTTGATCGCCGGCGTAATGGTTCCTA**CATGACAT**TATAATTAACTAAGATC-5′;
- Mutant sense: 5′-pAAACTAGCGGCCGCATTACCAAGGAT**TTTTTTTTT**ATATTAATTGATTCTAG-3′;
- Mutant antisense: 3′-pTTTGATCGCCGGCGTAATGGTTCCT**AAAAAAAAA**TATAATTAACTAAGATC-5′.

C2C12 myoblasts (ATCC® CRL1772™, LGC Standards, Wesel, Germany) were seeded at 2×10^5 cells per well in white-walled 96-well plates. After 24 h, cells were co-transfected with 150 ng of the wild-type or mutant *PROX1* 3′UTR reporter together with 20 nM miR-101 mimic (agomiR; mirVana™ miRNA mimic, Life Technologies, Darmstadt, Germany) or scrambled negative control (NC; Life Technologies, Darmstadt, Germany). Lipofectamine 2000 (Life Technologies, Darmstadt, Germany) was used for transfection. Reporter activity was measured after 24 and 48 h using the Nano-Glo dual-luciferase reporter assay (Promega, Walldorf, Germany), and relative luciferase activity was calculated as NanoLuc/Firefly activity. Four independent experimental replicates per group were used [10]. Because this reporter assay was performed in murine C2C12 cells rather than BMSC, it was used as a complementary sequence-specific test of the cloned bovine PROX1 3′UTR region and is considered separately from the BMSC functional findings.

2.2. Isolation of Fetal Bovine Muscle Satellite Cells

Primary bovine muscle satellite cells (BMSCs) were isolated from skeletal muscle collected from the left foreleg of a Holstein–Friesian fetus at approximately 4.5 months of gestation. The bovine muscle satellite cells used in the present study were involved in the same previously established cell preparation described by Will et al. [29]. The cell preparation was achieved using the same isolation procedure described for our previous experiments with this bovine satellite-cell model [10]. Briefly, muscle tissue was finely minced in phosphate-buffered saline (PBS; 144 mM NaCl, 5.4 mM KCl, 25 mM glucose,

14 mM sucrose, 5 mM Na_2HPO_4, 50 IU/mL penicillin, 50 µg/mL streptomycin and 1 µg/mL phenol red; pH 7.4) and enzymatically dissociated with 0.3% trypsin (Invitrogen, Karlsruhe, Germany) for 1 h at 37 °C under continuous agitation. Digestion was terminated with addition of 20% fetal bovine serum (FBS; Invitrogen, Karlsruhe, Germany).

The resulting suspension was sequentially passed through sterile nylon meshes with pore sizes of 63 µm and 20 µm, diluted with PBS and centrifuged at 250× *g* for 10 min at 4 °C. Viable cells were determined by trypan-blue exclusion using a Neubauer counting chamber (Roth, Karlsruhe, Germany). Cells were initially plated at approximately 1×10^5 cells/cm^2 in 100 mm Primaria culture dishes (Falcon, Becton Dickinson, Heidelberg, Germany) and maintained in Dulbecco's Modified Eagle Medium (DMEM) supplemented with 0.02 M glutamine (Serva, Heidelberg, Germany), 10% FBS, 100 IU/mL penicillin and 100 µg/mL streptomycin at 37 °C under 6% CO_2. Expanded cells were detached using 0.05% trypsin/0.02% EDTA (Roth, Karlsruhe, Germany) and cryopreserved in DMEM containing 20% FBS and 10% dimethyl sulfoxide (DMSO; Serva, Heidelberg, Germany) until subsequent experiments. All BMSC experiments used cells derived from this single fetal donor; therefore, the independent replicates described below represent independent culture/transfection experiments rather than independent animals.

2.3. Cell Culture, Myogenic Differentiation and miR-101 Manipulation

For differentiation experiments, BMSC were plated at 1×10^4 cells per well in 6- or 12-well culture plates coated with Matrigel (Corning, New York, NY, USA). Cells were expanded in DMEM containing 10% FBS and 100 IU/mL penicillin–streptomycin at 37 °C and 6% CO_2. When cultures reached approximately 90% confluence, myogenic differentiation was initiated by replacing the growth medium with DMEM containing 2% FBS and 100 IU/mL penicillin–streptomycin (PAN-Biotech, Aidenbach, Germany). Differentiation medium was changed every second day. For temporal expression analysis, cells were collected immediately before induction of differentiation (day 0) and after 1, 3 and 5 days. The time-course experiment was used to define the changing expression pattern across differentiation, whereas day 3 was selected for functional myotube endpoints because differentiated myotubes were established by this stage in the same BMSC workflow and this time point was used in the parallel experimental study [10].

For functional experiments, cellular miR-101 abundance was increased using a miR-101 mimic (agomiR; #MC11414, mirVana™ miRNA mimic, Thermo Fisher Scientific, Schwerte, Germany) or suppressed using a miR-101 inhibitor (antagomiR; #AM11414, Anti-miR™ miRNA Inhibitor, Thermo Fisher Scientific, Schwerte, Germany). Corresponding scrambled oligonucleotides served as negative control (NC). Oligonucleotides were used at 20–50 nM, depending on the experiment, consistent with the parallel experimental workflow [10], and were introduced at the onset of differentiation using Lipofectamine 2000 (Thermo Fisher Scientific, Schwerte, Germany) in Opti-MEM I reduced-serum medium. Cells were harvested on differentiation day 3 for RNA, protein and immunocytochemical analyses. Transfection efficacy was verified by quantifying miR-101 abundance relative to U6.

For lipid-accumulation experiments, day-3 myotubes were exposed to DMEM containing 2% fatty-acid-free bovine serum albumin and 500 µM oleic acid (dissolved in ethanol and conjugated to BSA) for 24 h in the presence of agomiR, antagomiR or NC [10].

2.4. RNA Extraction and Quantitative Real-Time PCR

Total RNA was extracted from cultured cells using QIAzol Lysis Reagent (Qiagen, Hilden, Germany) following the manufacturer's protocol. RNA concentration and purity were assessed with a NanoDrop 1000 spectrophotometer (Peqlab, Erlangen, Germany). For analysis of mRNA expression, 1 µg total RNA was reverse-transcribed using the cDNA

synthesis procedure employed previously in this cell system [10] with reagents from Bio-Rad (Munich, Germany).

Quantitative real-time PCR was carried out using SYBR Green chemistry on a LightCycler® 96 real-time PCR system (Roche, Basel, Switzerland). Each 20 µL reaction contained 10 ng cDNA and the appropriate gene-specific primer pair, and samples were analyzed in duplicate. Amplification consisted of an initial denaturation at 95 °C for 3 min followed by 45 cycles at 95 °C for 10 s, 60 °C for 30 s and 70 °C for 45 s. Relative transcript abundance was calculated using the $2^{-\Delta Ct}$ method [30]. GAPDH expression remained stable across the examined BMSC differentiation time points and was also used as the reference gene in the parallel experimental workflow [10]. The mitochondrial 16S/*HK2* ratio was analyzed separately, using *HK2* as the nuclear comparator for the mitochondrial 16S target, following the parallel workflow [10]. Primer sequences for *PROX1*, *MYOG*, *MYOD*, 16S, *HK2*, *COX7A2*, *TFAM*, *CPT1B*, *CD36*, *ACADM*, *FABP3*, *FABP4*, *ELOVL6*, *ACC2* and *GAPDH* are provided in Table 1.

Table 1. Primer sequences used for quantitative PCR. Primers for *MYOG*, *MYOD*, *16S*, *HK2*, *COX7A2*, *TFAM*, *CPT1B*, *CD36*, *ACADM*, *ELOVL6*, *ACC2*, *FABP3*, *FABP4* and *GAPDH*, were same as used in [10].

Gene	Accession Number	Forward Primer (5′–3′)	Reverse Primer (5′–3′)	Product (bp)
PROX1	NM_001193232.1	GGTGGGGAGGTCAGACAATG	GGCCGAGAAGACTTTGACCA	247
MYOG	NM_001111325.1	TGGGCGTGTAAGGTGTGTAA	TGCAGGCGCTCTATGTACTG	197
MYOD	NM_001040478.2	TTTGCCAGAGCAGGAGCCCCTC	TTCGAACACCTGAGCGAGCGC	123
16S	NC_006853.1	CTTGTATGAATGGCCGCACG	GATGTAGCGGGTCGTAGTGG	879
HK2	XM_015473383.2	CTCAGAGCGGCTCAAGACAA	GCACACCTCCTTGACGATGA	154
COX7A2	NM_175807.1	ACTGAGCCAAGATGCTACGG	TGAAGCCACAGCCAGTTCAT	242
TFAM	NM_001034016.2	GGCAGACTGGCAGGTATACAA	TGTGATGTGCCATCCCTAGC	225
CPT1B	NM_001034349.2	CTCTCCACTAGCCAGATCGC	CGCTGGGCATTTGTCTCTGA	197
CD36	NM_001278621.1	GACGGATGTACAGCGGTGAT	GGTTGCCAAGAGGTCTGGTT	250
ACADM	NM_001075235.1	CATGATCGCGCTGTTTAGGC	CAGGGTACTCGCCGGTTTTA	224
FABP3	NM_174313	GCGTTCTCTGTCGTCTTTCC	CTTGGTCATATTGCCCACCT	154
FABP4	NM_174314.2	GGATGGAAAATCAACCACCA	TGGACAACGTATCCAGCAGA	174
ELOVL6	NM_001102155.1	CATAGCACAGCCTCGGTCTA	TGCTGTGTCCTACCCCATTT	172
ACC2	NM_001205333.2	TCATTCACCTCCTGTCCACC	TAAACAGGAGTGAGCTGGGG	196
GAPDH	NM_001034034.2	GGGTCATCTCTGCACCT	ACAGTCTTCTGGGTGGCAGT	208

2.5. Measurement of miR-101 Expression

Cellular miR-101 abundance was determined using a TaqMan-based miRNA assay according to the procedure previously established for bovine muscle satellite cells [10,31]. Briefly, 50 ng total RNA was reverse-transcribed using the TaqMan MicroRNA Reverse Transcription Kit (Applied Biosystems, Carlsbad, CA, USA) together with a miRNA-specific stem-loop reverse-transcription primer. Reverse transcription was performed at 16 °C for 30 min and at 42 °C for 30 min, followed by enzyme inactivation at 85 °C for 5 min.

Quantitative PCR was subsequently performed using TaqMan Universal Master Mix II without UNG (Applied Biosystems, Carlsbad, CA, USA). Cycling conditions consisted of 10 min at 95 °C followed by 40 cycles of 95 °C for 15 s and 60 °C for 60 s. Reactions were analyzed in triplicate using a LightCycler 96 instrument (Roche, Basel, Switzerland). The TaqMan™ small nuclear RNA (snRNA) U6 control assay was used as a normalizing control.

2.6. Protein Extraction and Quantification

Protein abundance was analyzed using conventional Western blotting for *PROX1* and an automated capillary-based Simple Western system (Jess, Bio-Techne, San Jose, CA, USA) for the remaining proteins. Cell monolayers were rinsed with ice-cold PBS and lysed in CelLytic MT reagent supplemented with Protease Inhibitor Cocktail (Sigma-Aldrich, Munich, Germany). After centrifugation at 14,000 rpm for 15 min, clarified lysates were collected and adjusted to a protein concentration of 1 mg/mL.

A PROX1-immunoreactive band was detected after protein separation on Criterion TGX stain-free gels (Bio-Rad, Munich, Germany) and transfer to polyvinylidene difluoride (PVDF) membranes using Trans-Blot Turbo transfer packs and a Trans-Blot semi-dry blotter (Bio-Rad, Munich, Germany). After blocking for 1 h with 5% BSA in TBST, membranes were incubated with the primary antibody overnight at 4 °C. An HRP-conjugated secondary antibody (TrueBlot rabbit, 1:10,000) and SuperSignal West Femto chemiluminescence substrate (Thermo Scientific) were used for detection. Chemiluminescence was recorded with a ChemoCam HR-16 imager (INTAS, Göttingen, Germany) and quantified using LabImage 1D software, version 4.2.1 (Kapelan Bio-Imaging, Leipzig, Germany). AKT, *MYOG*, MYH7 and MYH8 were quantified using the Jess Simple Western system and the 12–230 kDa Separation Module (Bio-Techne). The antibody working dilutions were 1:40 for AKT, 1:25 for *MYOG* and 1:50 for MYH7 and MYH8 [10]. Antibodies and working dilutions are summarized in Table 2.

Table 2. Immunodetection targets and working dilutions documented in the parallel bovine muscle-cell workflow.

Target	Application	Working Dilution	Source/Detail
PROX1	Western blot/immunocytochemistry	1:1000/1:100	Abcam (Cambridge, UK), ab101851
AKT	Jess Simple Western	1:40	As used in parallel study [10]
MYOG	Jess Simple Western	1:25	As used in parallel study [10]
MYH7	Jess Simple Western	1:50	As used in parallel study [10]
MYH8	Jess Simple Western	1:50	As used in parallel study [10]
MYOG	Immunocytochemistry	1:100	Abcam, ab1835 [10]
MYH7	Immunocytochemistry	1:100	antibodies-online, ABIN3043105 [10]
MYH8	Immunocytochemistry	1:100	Abcam, ab210947 [10]

Quantitative values for the Jess targets were derived from the instrument-generated capillary electrophoresis/chemiluminescence signals processed in Compass software and were normalized to total protein measured in the same capillaries using the RePlex procedure and Total Protein Assay (Bio-Techne). The virtual band images are representative visualizations generated from the capillary data and were not manually densitometrically quantified from the rasterized figure image. Electropherograms and quantitative data were processed using Compass for Simple Western software, version 6.0.0, Build 0408 (Bio-Techne).

2.7. Immunocytochemistry

Immunocytochemistry was performed on differentiated BMSC to examine PROX1 and selected markers of myogenic differentiation and fiber phenotype. Cells were washed with PBS, fixed in 4% paraformaldehyde and permeabilized with PBS containing 0.1% Triton

X-100 (Sigma-Aldrich, Munich, Germany). Non-specific binding was blocked using 10% normal goat serum before overnight incubation with primary antibodies at 4 °C.

PROX1 (Abcam, ab101851), MYOG (Abcam, ab1835), MYH7 (antibodies-online, ABIN3043105) and MYH8 (Abcam, ab210947) antibodies were applied at a dilution of 1:100. After washing, cells were incubated for 45 min at room temperature with the appropriate Alexa Fluor 488 goat-anti-rabbit IgG or Alexa Fluor 594 goat-anti-mouse IgG secondary antibody at 1:500 (Thermo Fisher Scientific, Schwerte, Germany). Nuclei were visualized using Hoechst 33258 (Sigma-Aldrich, Munich, Germany), and preparations were mounted with ProLong Diamond Antifade Mountant (Thermo Fisher Scientific, Schwerte, Germany).

Fluorescence images were acquired using a Nikon Microphot SA microscope (Nikon, Düsseldorf, Germany) equipped with a CC-12 color camera (OSIS, Münster, Germany). Image evaluation was performed using Cell^F software, version 3.4, build 1175 (OSIS, Münster, Germany). Color intensity and saturation were quantified in seven images per treatment as semi-quantitative descriptors of the immunofluorescence signal. Intensity was used to summarize fluorescence brightness, whereas saturation was included to describe the chromatic strength of the marker-specific staining independent of brightness. These image-based measurements were interpreted together with, rather than as a replacement for, the protein-abundance measurements.

2.8. BrdU Proliferation Assay

The influence of miR-101 manipulation on myoblast proliferation was assessed by incorporation of 5-bromo-2′-deoxyuridine (BrdU). This assay was intentionally performed in proliferating myoblasts before induction of differentiation, rather than in day-3 myotubes, because BrdU incorporation was used specifically to assess DNA synthesis during proliferation. BMSC were seeded at 0.5×10^4 cells per well and, after 24 h, incubated with 10 µM BrdU (ab142567; Abcam, Cambridge, UK) for 4 h at 37 °C. Three wells were evaluated per treatment. Cells were subsequently fixed in 4% paraformaldehyde and permeabilized with PBS containing 0.1% Triton X-100 (Sigma-Aldrich, Munich, Germany). Incorporated BrdU was exposed by incubation with 2 N HCl for 20 min at 37 °C. After blocking with 10% normal goat serum, cells were incubated overnight at 4 °C with an anti-BrdU antibody (1:100; Roche, Mannheim, Germany). BrdU-positive nuclei were detected with Alexa Fluor 488 goat-anti-mouse IgG (1:500; Thermo Fisher Scientific, Schwerte, Germany), while total nuclei were counterstained with propidium iodide (5 µg/mL).

Images were acquired with a Nikon Microphot SA microscope (Nikon, Düsseldorf, Germany) and CC-12 camera (OSIS, Münster, Germany). BrdU-positive and total nuclei were counted using Cell^F software (OSIS, Münster, Germany) in 10 randomly selected fields per sample, corresponding to a total analyzed area of 10.7 mm^2. Proliferation was expressed as the percentage of BrdU-positive nuclei relative to total nuclei.

2.9. Oil Red O Staining and Image Analysis

Intramyocellular neutral-lipid accumulation was evaluated following 24 h of oleic-acid exposure. Myotubes were rinsed twice with pre-warmed PBS and fixed for 30 min at room temperature with 4% paraformaldehyde (Roth, Karlsruhe, Germany). Fixed cultures were equilibrated in 60% isopropanol for 5 min and subsequently incubated with freshly prepared Oil Red O working solution for 5 min. Excess stain was removed by repeated rinsing with distilled water. Wells were covered with gelatin (Waldeck, Münster, Germany) and coverslips (Roth, Karlsruhe, Germany).

Oil Red O-stained cultures were examined using a Nikon Diaphot 300 inverted phase-contrast microscope (Nikon, Düsseldorf, Germany) equipped with a CC-12 camera (OSIS, Münster, Germany). Quantitative image analysis was carried out with Cell^F software (OSIS, Münster, Germany) using the previously established image-analysis macro [32,33]. The parameters quantified were lipid-particle number per unit area, mean distance between lipid particles, and percentage of image area occupied by lipid and mean lipid-particle size. Twenty images were evaluated from each well, corresponding to a total analyzed area of 8.3 mm^2.

2.10. Statistical Analysis

Statistical analyses were performed with SAS version 9.4 (SAS Institute Inc., Cary, NC, USA). All primary-cell experiments used BMSC derived from the same fetal donor. Thus, an independent experimental replicate denotes a separate culture experiment, including a separate plating and, where applicable, a separate miRNA transfection, rather than an independent animal. The differentiation time course comprised four independent experimental replicates per time point; miR-101 gain- and loss-of-function and BrdU assays comprised three independent experimental replicates per group; lipid-related gene-expression analyses comprised two or three independent experimental replicates per group, depending on the endpoint. Technical qPCR duplicates or triplicates were averaged within each independent experiment before statistical analysis. Treatment effects were evaluated using one-way analysis of variance or the general linear model procedure, as appropriate. Treatment or differentiation day was included as the fixed effect, and results are reported as means ± standard error of the mean (SEM). Where an overall effect was detected, Tukey's test was used for pairwise comparisons.

Gene and protein expression data were expressed relative to the appropriate negative-control treatment or differentiation day-0 reference. Values of miR-101 expression, obtained after agomiR or antagomiR treatment, were logarithmically transformed before analysis to improve homogeneity of variance. Differences were considered statistically significant at $p < 0.05$, whereas $0.05 < p < 0.10$ was considered indicative of a statistical trend. For the Oil Red O image-analysis data, overall treatment p values are reported in the results, and direct pairwise significance comparisons are shown in the corresponding graphical presentation.

3. Results

3.1. Heterologous Reporter Assay Shows miR-101 Responsiveness of the Bovine PROX1 3′UTR Seed-Matching Site

Sequence analysis identified a conserved predicted miR-101 seed-matching site at positions 5077–5084 of the bovine *PROX1* 3′UTR (Figure 1a). In the heterologous C2C12 reporter system, co-transfection of miR-101 agomiR with the wild-type *PROX1* 3′UTR reporter reduced relative luciferase activity by approximately 33% at 24 h ($p < 0.001$) and 31% at 48 h ($p < 0.01$) compared with the negative control (Figure 1b). Replacement of the wild-type seed-matching sequence 5′-GTACTGTA-3′ by the mutant poly-T segment 5′-TTTTTTTTT-3′ abolished this repressive response. Thus, the cloned bovine *PROX1* 3′UTR sequence was responsive to miR-101 in C2C12 cells. This finding is interpreted as a sequence-specific response in the heterologous C2C12 reporter system.

(a)

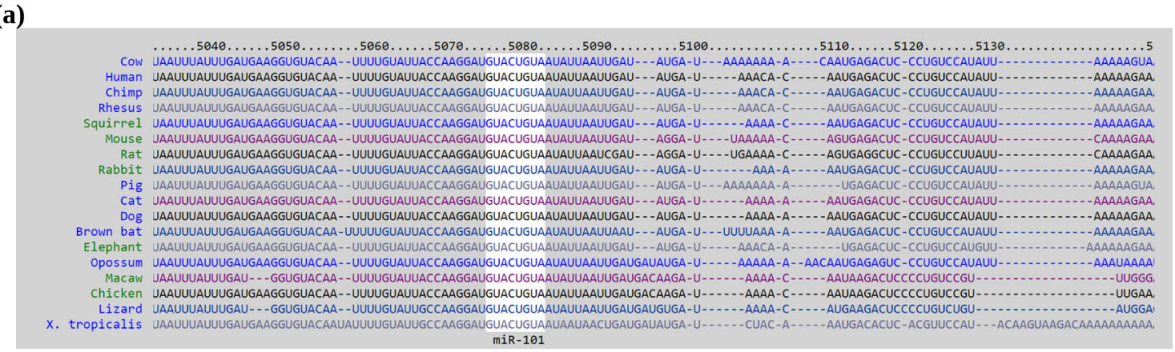

Position 5077-5084 of PROX1 3' UTR	5' ...UGUAUUACCAAGGAUGUACUGUA...
	|||||||
bta-miR-101	3' AAGUCAAUAGUGUCAUGACAU

(b)

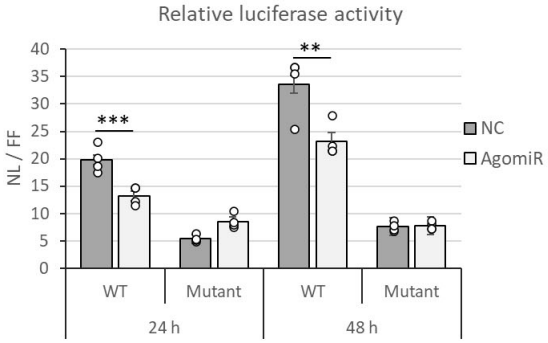

Figure 1. Predicted miR-101 seed-matching site and reporter response of the bovine *PROX1* 3′UTR. (**a**) Conservation of the target-region sequence across vertebrate species and predicted pairing of bta-miR-101 with the bovine *PROX1* 3′UTR seed-matching site at positions 5077–5084. The miR-101 seed region and the complementary seed-matching site in the *PROX1* 3′UTR are indicated. In the mutant reporter, the wild-type target-site seed-matching sequence 5′-GTACTGTA-3′ was replaced by the poly-T segment 5′-TTTTTTTT-3′ to disrupt complementarity to the miR-101 seed. (**b**) Dual-luciferase reporter assay in C2C12 cells after co-transfection of miR-101 agomiR or negative control (NC) with wild-type (WT) or seed-matching-site-mutated *PROX1* 3′UTR reporters. Relative NanoLuc/Firefly (NL/FF) activity is shown at 24 and 48 h. Data represent four independent experimental replicates per group and are shown as mean ± SEM. ** $p < 0.01$; *** $p < 0.001$.

3.2. miR-101 and PROX1 Show Reciprocal Temporal Expression During Myogenic Differentiation

The expression of miR-101 and *PROX1* was monitored during the differentiation of primary bovine muscle satellite cells (Figure 2). Relative to day 0, miR-101 abundance decreased by approximately 31% on day 1, followed by increases of approximately 10% and 36% on days 3 and 5, respectively. miR-101 expression on day 5 was significantly higher than on day 1 ($p < 0.05$; Figure 2a). In contrast, *PROX1* mRNA showed an opposite temporal pattern, increasing by approximately 570% on day 1 relative to day 0 ($p < 0.01$; Figure 2b), followed by lower expression on days 3 and 5, which nevertheless remained approximately 230% and 100% above the day-0 level, respectively. *PROX1* expression was significantly lower on days 3 and 5 than on day 1 ($p < 0.05$; Figure 2b). These opposite temporal patterns describe an inverse temporal association between miR-101 and *PROX1* during myogenic differentiation.

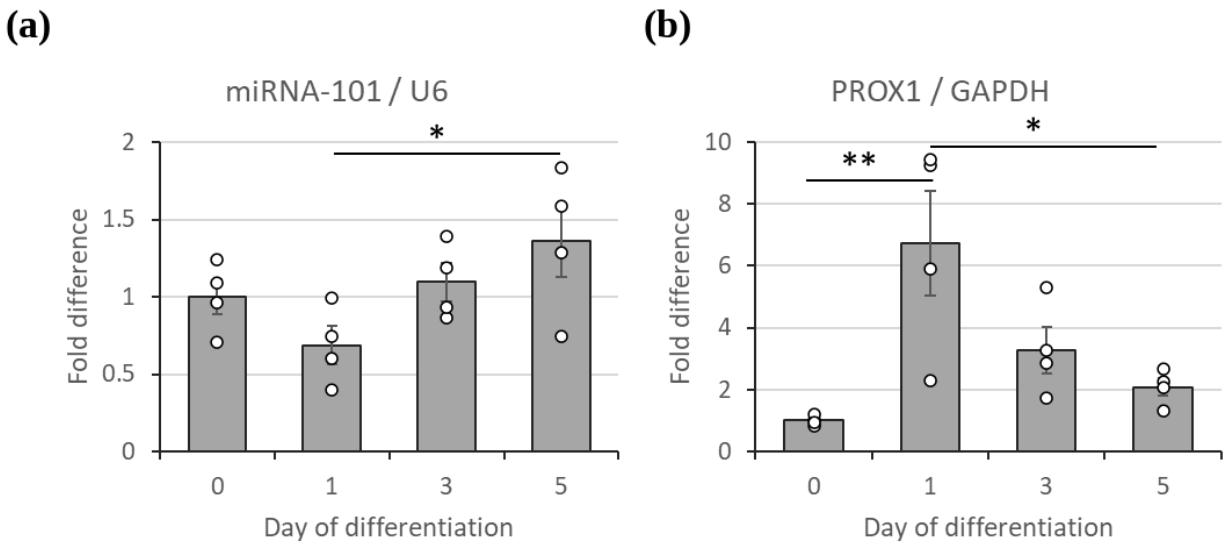

Figure 2. miR-101 and *PROX1* expression during bovine muscle satellite-cell differentiation. (**a**) miR-101 abundance normalized to U6 and (**b**) *PROX1* mRNA normalized to *GAPDH* across days 0, 1, 3 and 5 of differentiation. Data represent four independent experimental replicates per time point and are shown as mean ± SEM relative to day 0. * $p < 0.05$; ** $p < 0.01$ for the indicated comparisons.

3.3. miR-101 Gain- and Loss-of-Function Effects on PROX1 and Myogenic-Marker Profiles

The effectiveness of miR-101 gain- and loss-of-function was confirmed by an approximately 870-fold increase in miR-101 abundance after agomiR treatment ($p < 0.001$; Figure 3a) and an approximately 85% reduction after antagomiR treatment ($p < 0.05$; Figure 3d). Despite this robust manipulation of miR-101, neither *PROX1* mRNA abundance nor the PROX1-immunoreactive signal differed significantly from the respective negative control after agomiR or antagomiR treatment (Figure 3b,c,e,f). Mean *PROX1* values were lower after agomiR and higher after antagomiR treatment, but neither difference was statistically significant.

Among the myogenic markers, agomiR treatment significantly increased MYOG mRNA abundance by approximately 90% ($p < 0.05$; Figure 3b), whereas MYOD mRNA was not significantly changed. At the protein level, AKT, MYOG, MYH7 and MYH8 did not differ significantly after agomiR treatment (Figure 3c,i). Following antagomiR treatment, MYOG protein showed a statistical trend toward higher abundance ($0.05 < p < 0.10$; Figure 3f,i), while the other measured mRNA and protein markers were not significantly altered. Thus, downstream myogenic markers did not show a uniform reciprocal response to miR-101 gain- versus loss-of-function.

Immunocytochemical staining confirmed the presence of PROX1 and the myogenic markers MYOG, MYH7 and MYH8 in differentiated cells across all treatment groups (Figure 3g). Quantitative image analysis detected no significant overall treatment effect on fluorescence color intensity, although intensity tended to be lower in agomiR-treated than antagomiR-treated cells ($p = 0.068$; Figure 3h). Color saturation of MYH7 and MYH8 was significantly higher in antagomiR-treated cells ($p < 0.05$; Figure 3h), providing additional evidence of treatment-related differences in myotube staining characteristics.

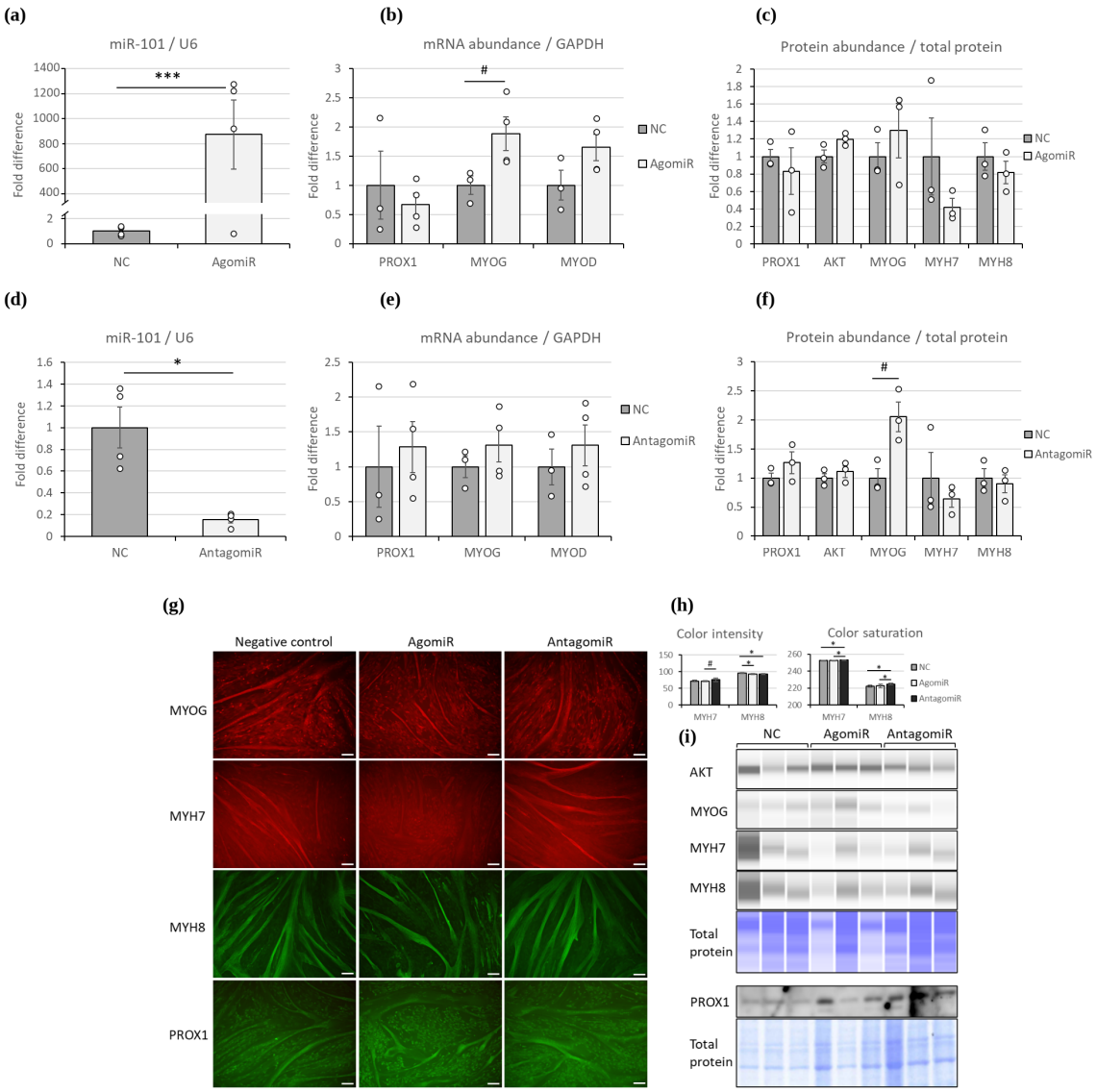

Figure 3. Effects of miR-101 overexpression and inhibition on *PROX1* expression and myogenic markers in bovine muscle satellite-cell-derived myotubes. (**a**) Relative miR-101 abundance following agomiR treatment compared with the corresponding negative control (NC). (**b**) Relative mRNA abundance of *PROX1*, *MYOG* and *MYOD* after miR-101 overexpression. (**c**) Relative PROX1-immunoreactive signal and protein abundance of AKT, *MYOG*, MYH7 and MYH8 following agomiR treatment. (**d**) Relative miR-101 abundance following antagomiR treatment compared with NC. (**e**) Relative mRNA abundance of *PROX1*, *MYOG* and *MYOD* after miR-101 inhibition. (**f**) Relative PROX1-immunoreactive signal and protein abundance of AKT, *MYOG*, MYH7 and MYH8 following antagomiR treatment. (**g**) Representative immunocytochemical images of *MYOG*, MYH7, MYH8 and *PROX1* in NC-, agomiR- and antagomiR-treated BMSC myotubes. Scale bars represent 100 µm. (**h**) Quantification of immunocytochemical color intensity and saturation from seven images per treatment; bars represent mean ± SEM. (**i**) Representative virtual Simple Western images for AKT, *MYOG*, MYH7 and MYH8 and conventional Western blot images for *PROX1*. Quantitative values for Jess targets were obtained from Compass analysis of capillary signals normalized to total protein; the virtual band images are representative visualizations and were not manually quantified from the displayed image. Molecular-expression data represent three independent experimental replicates per group and are shown as mean ± SEM relative to the corresponding negative control. miR-101 was normalized to U6, mRNA expression to *GAPDH* and protein abundance to total protein. * $p < 0.05$; *** $p < 0.001$; #, statistical trend ($0.05 < p < 0.10$).

3.4. Altered miR-101 Abundance Does Not Significantly Affect Myoblast Proliferation

To determine whether the downstream phenotypes could be explained by changes in cell proliferation, BrdU incorporation was quantified relative to the total number of nuclei (Figure 4). Approximately half of the nuclei were BrdU-positive in control cultures, with marginally higher percentages after treatment with both agomiR and antagomiR. No significant differences were detected among treatments. Thus, increasing or inhibiting miR-101 did not substantially alter proliferation of bovine muscle satellite cells under these conditions.

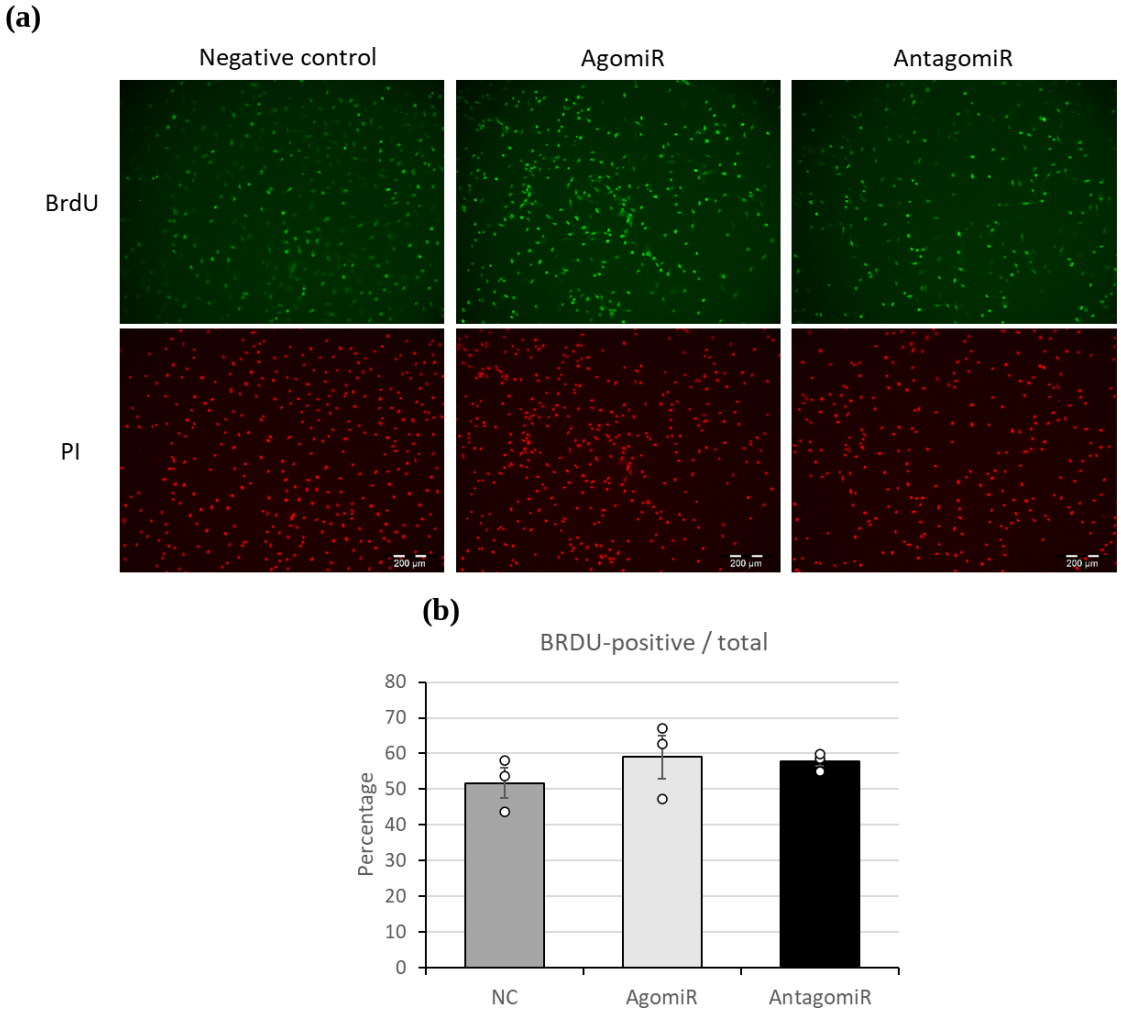

Figure 4. Effect of altered miR-101 abundance on bovine muscle satellite-cell proliferation. (**a**) BrdU-positive nuclei are shown in green and total nuclei stained with propidium iodide (PI) in red for negative-control (NC), agomiR and antagomiR treatments. Scale bars represent 200 µm. (**b**) BrdU-positive nuclei as a percentage of total nuclei. Data represent three independent experimental replicates per group and are shown as mean ± SEM. No significant treatment effect was observed.

3.5. miR-101 Perturbation Increases Intramyocellular Lipid Accumulation and Alters Lipid-Particle Characteristics

Oil Red O staining and quantitative image analysis showed increased neutral-lipid accumulation in oleic-acid-treated myotubes following both miR-101 overexpression and inhibition compared with the negative control (Figures 5a and 6; Table 3). Lipid-particle density increased by approximately 46% after both agomiR and antagomiR treatment ($p = 0.0035$). Mean interparticle distance decreased by approximately 11.9% and 11.2%,

respectively ($p = 0.0005$), while the lipid-covered area increased by approximately 35.8% with agomiR and 52.4% with antagomiR ($p = 0.0015$). For lipid-particle density, interparticle distance and lipid-covered area, both agomiR and antagomiR differed significantly from the negative control, whereas agomiR and antagomiR did not differ significantly from each other for these three parameters.

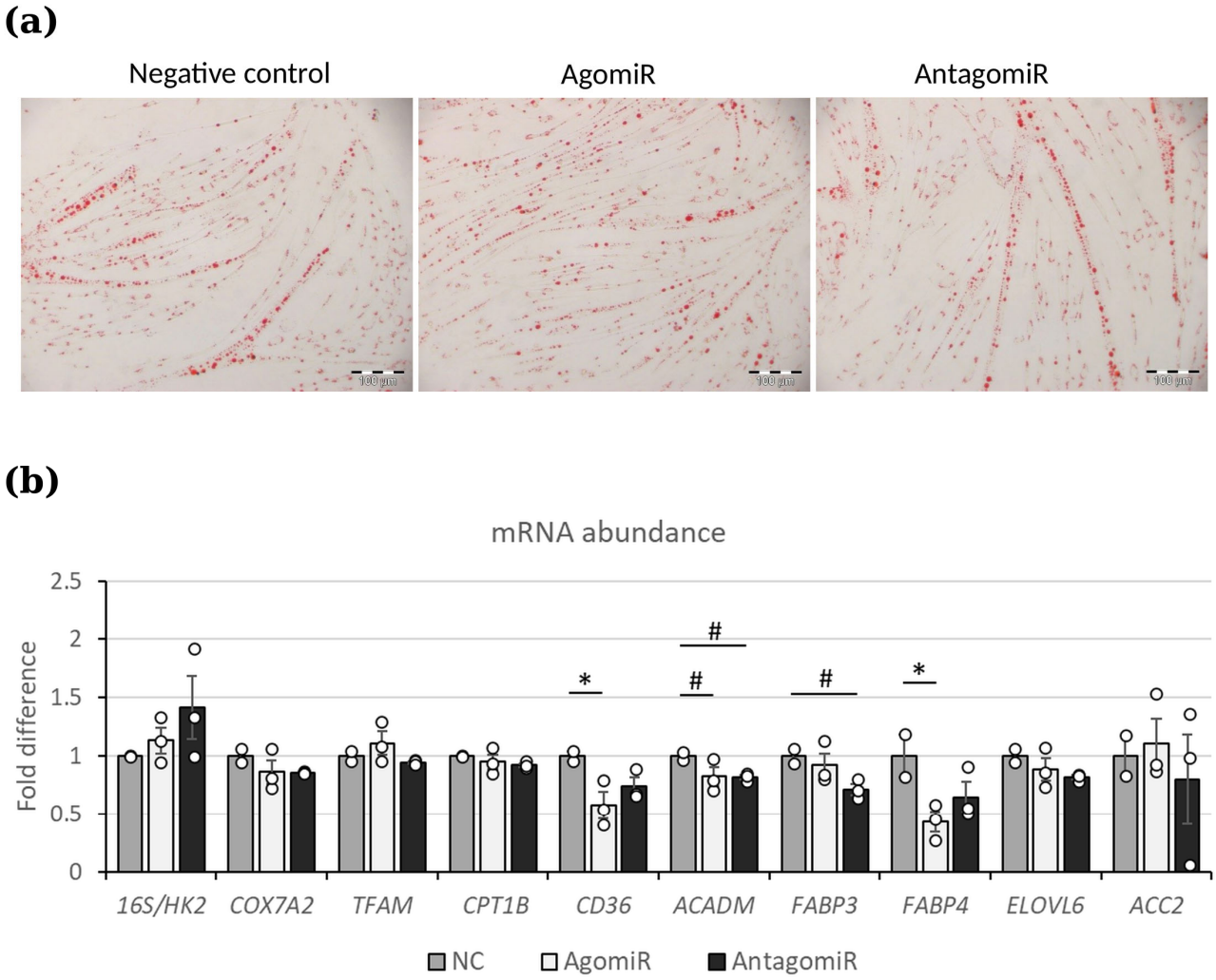

Figure 5. Effects of miR-101 manipulation on oleic-acid-induced intramyocellular lipid accumulation and metabolic gene expression in bovine myotubes. (**a**) Representative Oil Red O-stained myotubes treated with negative control (NC), agomiR or antagomiR plus oleic acid. Scale bars represent 100 µm. (**b**) Relative abundance of transcripts related to mitochondrial content/function, fatty-acid oxidation, transport and lipid handling. Expression was normalized to *GAPDH* except for the mitochondrial 16S/*HK2* ratio; *HK2* served as the nuclear comparator for the mitochondrial 16S target, following the parallel experimental workflow [10]. Gene-expression data represent two or three independent experimental replicates per group, depending on the endpoint, and are shown as mean ± SEM relative to NC. * $p < 0.05$; #, statistical trend ($0.05 < p < 0.10$).

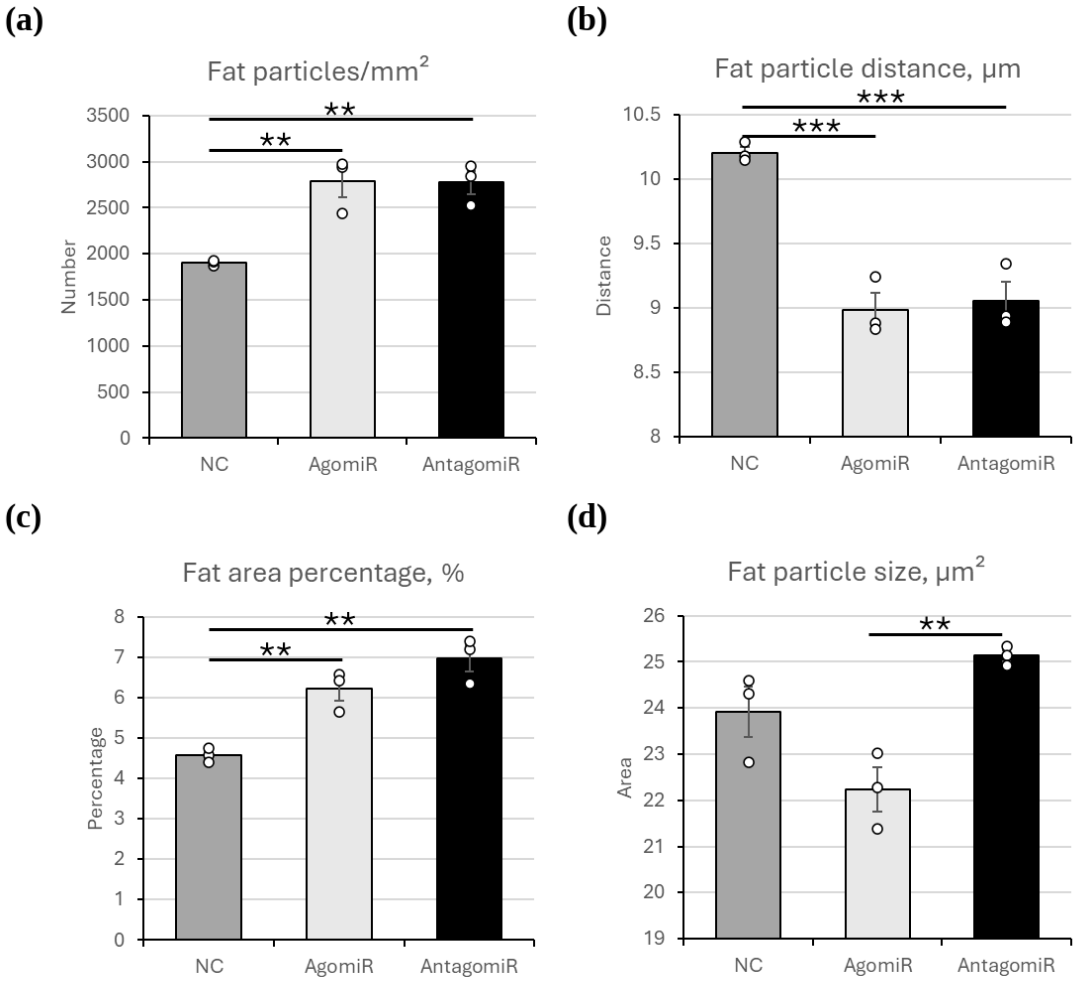

Figure 6. Graphical presentation of the Oil Red O image-analysis data summarized in Table 3. (**a**) Fat particle density; (**b**) mean interparticle distance; (**c**) lipid-covered area; (**d**) mean fat particle size in negative-control (NC), agomiR, and antagomiR treatments. Individual data points are shown, and bars represent mean ± SEM. ** $p < 0.01$; *** $p < 0.001$ for the indicated comparisons.

Table 3. Image analysis of Oil Red O-stained bovine satellite-cell myotubes after treatment with oleic acid and miR-101 agomiR or antagomiR compared with a negative control. Values are mean ± SEM. Overall treatment *p* values are shown in the table; direct pairwise significance comparisons are illustrated in Figure 6.

	Treatment						
	Negative Control		**AgomiR**		**AntagomiR**		***p*-Value**
	Mean	**SE**	**Mean**	**SE**	**Mean**	**SE**	
Fat particles/mm²	1904.9	18.1	2785.3	170.9	2773.2	127.4	0.0035
Fat particle distance, µm	10.20	0.04	8.99	0.13	9.06	0.14	0.0005
Fat area percentage	4.58	0.10	6.22	0.28	6.98	0.32	0.0015
Fat particle size, µm²	23.91	0.55	22.23	0.47	25.13	0.12	0.0084

Mean lipid-particle size also differed among treatments ($p = 0.0084$; Table 3). AgomiR-treated cells contained particles that were approximately 11.5% smaller than those in antagomiR-treated cells ($p < 0.05$), whereas the negative-control value was intermediate and did not differ significantly from either treatment. Thus, perturbing miR-101 in either direction increased overall intramyocellular lipid accumulation, while gain- and loss-of-function produced distinct lipid-particle size characteristics.

3.6. miR-101 Perturbation Selectively Alters Transcripts Involved in Fatty-Acid Handling

The transcriptional response accompanying lipid accumulation was selective rather than global (Figure 5b). Relative to the negative control, miR-101 overexpression reduced *CD36* and *FABP4* mRNA abundance by approximately 42% and 56%, respectively ($p < 0.05$). *ACADM* showed a downward statistical trend after both agomiR and antagomiR treatment, while *FABP3* tended to be lower after antagomiR treatment ($0.05 < p < 0.10$). No significant treatment effects were detected for *COX7A2, TFAM, CPT1B, ELOVL6, ACC2* or the mitochondrial 16S/HK2 ratio. Overall, miR-101 perturbation selectively affected transcripts involved in fatty-acid transport and handling rather than causing a generalized change in lipid-metabolic gene expression.

4. Discussion

The reporter assay supports a sequence-specific interaction between miR-101 and the bovine *PROX1* 3′UTR in C2C12 cells. While miR-101 and *PROX1* displayed reciprocal temporal expression during differentiation and despite robust gain- and loss-of-function manipulation, endogenous *PROX1* mRNA abundance and the PROX1-immunoreactive signal did not differ significantly. The miR-101 perturbation produced selective, non-uniform changes in myogenic markers. The clearest functional phenotype was increased oleic-acid-induced intramyocellular lipid deposition after both miR-101 overexpression and inhibition. Overall, in BMSC, miR-101 perturbation affected selected myogenic and lipid-related phenotypes, whereas endogenous *PROX1* mRNA abundance and the *PROX1*-immunoreactive signal were not significantly affected.

The reporter experiment is interpreted as a complementary sequence-specific observation from the heterologous C2C12 system. MicroRNA-101 reduced luciferase activity from the wild-type bovine *PROX1* 3′UTR at both measured time points, whereas disruption of the target-site sequence complementary to the miR-101 seed abolished repression, consistent with sequence-specific miRNA recognition [14,28]. However, the reporter assay was performed in murine C2C12 cells, whereas the endogenous experiments used primary bovine muscle satellite cells. Species and cell-context differences, including target abundance, RNA-binding proteins, competing transcripts and differentiation state, may influence whether a responsive 3′UTR sequence produces measurable endogenous regulation [14,15]. Accordingly, the reporter result is considered separately from the BMSC functional findings.

The differentiation time course provides a separate correlative observation. *PROX1* was strongly induced on day 1 when miR-101 was at its lowest level, and *PROX1* subsequently declined as miR-101 increased. This inverse pattern describes a temporal association between miR-101 and *PROX1* during differentiation. The temporal pattern of *PROX1* is biologically plausible because previous work in mice showed that *PROX1* is present in satellite cells, is induced during differentiation and contributes to a slow-fiber transcriptional program that includes MYH7 [11,12]. In the present BMSC experiments, however, miR-101 manipulation did not significantly change endogenous *PROX1* or MYH7 abundance. Therefore, the known role of *PROX1* in fiber-type regulation provides biological context for the candidate interaction but should not be interpreted as evidence that miR-101 drove fiber-type conversion in these cells.

The livestock context remains relevant to the biological question. In pigs, *PROX1* is more abundant in soleus than biceps femoris and its expression parallels myoglobin and type I myosin heavy chain while opposing a fast-fiber marker [13]. Because oxidative and glycolytic fiber programs differ in mitochondrial density, lipid utilization and contractile properties [2], *PROX1* represents a possible point of intersection between muscle differentiation, fiber identity and metabolism. In the present BMSC experiments, however, endogenous *PROX1* did not significantly change after miR-101 manipulation; therefore,

the established *PROX1* functions are discussed here in a biological context rather than as a miR-101-mediated mechanism in BMSC.

Consistent with this interpretation, no statistically significant differences in *PROX1* mRNA abundance or the *PROX1*-immunoreactive signal were detected after either agomiR or antagomiR treatment. Thus, under the present experimental conditions, miR-101 manipulation affected selected myogenic and lipid-related outcomes without a significant change in endogenous *PROX1*. An additional limitation is that the PROX1-immunoreactive band migrated at approximately 50–60 kDa, below the expected molecular mass of full-length PROX1 (approximately 83 kDa); therefore, its identity as full-length bovine PROX1 cannot be established noticeably from the present Western blot.

The myogenic-marker results also argue against a simple reciprocal model of miR-101 action. *MYOG* mRNA increased significantly after miR-101 overexpression, whereas *MYOG* protein showed only a statistical trend towards higher abundance after miR-101 inhibition. The other measured myogenic markers were not significantly changed. Thus, increasing and decreasing miR-101 did not produce mirror-image molecular responses. In C2C12 cells, Liu et al. reported that transiently upregulated miR-101a/b can act as a molecular brake on differentiation through multiple pathways and identified MEF2A as a direct target [20]. The primary bovine-cell response observed here may differ because of species, primary versus immortalized cell state, developmental origin, timing of manipulation, target-network composition and potential differences between transcript and protein kinetics. The absence of a significant effect on BrdU incorporation also argues against a large proliferation change as the explanation for these downstream patterns.

The most robust phenotype was the effect on neutral-lipid accumulation. Both agomiR and antagomiR increased lipid-particle density and lipid-covered area and reduced the distance between particles relative to the negative control. The two interventions nevertheless differed in particle size, with smaller average particles after agomiR than after antagomiR treatment and the control intermediate. This pattern indicates that opposite perturbations of miR-101 can produce a similar increase in total intracellular lipid while differing in the organization of lipid storage. Intramyocellular lipid abundance reflects the balance among fatty-acid uptake, esterification, lipid-droplet turnover and mitochondrial oxidation; similar total lipid accumulation can therefore arise through different underlying mechanisms [8,34,35].

The similar lipid-accumulation response to miR-101 overexpression and inhibition is inconsistent with a simple linear model in which one direction of miR-101 change produces one opposite lipid phenotype. Individual miRNAs can regulate multiple transcripts and participate in feedback networks [14,15]; consequently, agomiR and antagomiR treatment may perturb different combinations of direct targets and compensatory pathways. A homeostatic response to moving miR-101 above or below its physiological range is also possible. In addition, synthetic miRNA mimics and inhibitors can produce non-physiological or off-target effects, which cannot be excluded in the present experiments. The significantly different particle size between agomiR and antagomiR further suggests that the cellular routes leading to increased storage were not identical. The current data do not distinguish among these possibilities, and they should therefore be considered mechanistic hypotheses rather than demonstrated explanations.

The metabolic-gene data provide additional context but not a complete mechanism. AgomiR significantly reduced *CD36*, which contributes to long-chain fatty-acid transport, and *FABP4*, a lipid-binding protein, while *ACADM* and *FABP3* showed downward trends. Several other measured transcripts, including *COX7A2*, *TFAM*, *CPT1B*, *ELOVL6* and *ACC2*, were not significantly different. The coexistence of increased lipid storage with reduced *CD36* and *FABP4* expression further argues against a simple explanation based only on

increased fatty-acid uptake and may reflect compensatory transcriptional responses. Direct measurements of oxygen consumption, radiolabeled fatty-acid oxidation, acyl-carnitines or mitochondrial respiratory function would be required to determine whether lipid oxidation was altered.

These findings should also be interpreted carefully in relation to bovine IMF. The discovery cohort measured gene and miRNA expression in intact longissimus dorsi muscle differing in IMF [26], whereas the present in vitro assay measures neutral lipid stored inside differentiated muscle cells after oleic-acid exposure. Whole-muscle IMF includes lipid in intramuscular adipocytes as well as intracellular lipid within myofibers [6,7]. Consequently, the current experiments model the muscle-cell component of lipid handling but do not demonstrate effects on intramuscular adipocyte differentiation, whole-muscle IMF or marbling. Moreover, intact muscle contains additional cell types and endocrine, paracrine and metabolic inputs that may modify miR-101-dependent effects observed in vitro. A further limitation is that the primary BMSC originated from a single fetal donor; independent replicates were separate culture/transfection experiments and therefore do not capture between-animal biological variability. Although GAPDH showed no apparent variation across the examined differentiation series, its stability was not independently validated against an alternative reference gene; this should be considered when interpreting temporal expression changes. Validation in cells from multiple animals, with validated reference genes and in vivo models, will be required to establish the generality and physiological relevance of these findings.

5. Conclusions

In primary fetal BMSC undergoing myogenic differentiation, manipulation of miR-101 abundance altered the expression of selected genes involved in myogenic differentiation and lipid handling, including *MYOG*, *CD36* and *FABP4*, while endogenous *PROX1* mRNA abundance and the *PROX1*-immunoreactive signal were not significantly affected. These findings indicate that miR-101 influences selected myogenic and lipid-related gene-expression responses in differentiating BMSC under the present experimental conditions.

Author Contributions: Conceptualization, S.M. and B.A.M.; methodology, B.A.M., E.A., A.A. and S.M.; investigation, B.A.M., E.A. and A.A.; data curation and analysis, B.A.M., E.A., A.A. and K.S.; interpretation of data and results, B.A.M., E.A., A.A., K.S., S.S., M.A., M.P.G., O.H. and S.M.; scientific input on PROX1 biology and interpretation of the PROX1-related findings, S.S. and O.H.; scientific input on microRNA biology and interpretation of the miR-101-related findings, M.A. and A.A.; interpretation of the myogenic data, K.S., O.H., E.A. and S.M.; interpretation of the lipid-metabolism and intramyocellular lipid findings, M.P.G., K.S., B.A.M. and E.A.; writing—original draft preparation, B.A.M., E.A. and S.M.; writing—review and critical revision for important intellectual content, B.A.M., E.A., A.A., K.S., S.S., M.A., M.P.G., O.H. and S.M. All authors have read and agreed to the published version of the manuscript.

Funding: This research received no external funding.

Institutional Review Board Statement: The present study was conducted entirely in vitro using previously established primary bovine muscle satellite cells isolated from skeletal muscle of a Holstein–Friesian fetus at approximately 4.5 months of gestation, as originally described by Will et al. [29]. The same cell preparation was subsequently used in our previous study [10]. No additional animals were used, and no new animal tissue collection was performed specifically for the present study.

Informed Consent Statement: Not applicable.

Data Availability Statement: Data presented in this manuscript are available upon reasonable request to the corresponding author, with the exception of sensitive data according to GDPR current regulations.

Acknowledgments: We thank E. Schwitulla, S. Foß, and A. Berndt for expert technical assistance. We are grateful to Siriluck Ponsuksili for providing lab access and reagents.

Conflicts of Interest: The authors declare no conflicts of interest.

References

1. Chargé, S.B.P.; Rudnicki, M.A. Cellular and molecular regulation of muscle regeneration. *Physiol. Rev.* **2004**, *84*, 209–238. [CrossRef] [PubMed]
2. Schiaffino, S.; Reggiani, C. Fiber types in mammalian skeletal muscles. *Physiol. Rev.* **2011**, *91*, 1447–1531. [CrossRef] [PubMed]
3. Matarneh, S.K.; Silva, S.L.; Gerrard, D.E. New insights in muscle biology that alter meat quality. *Annu. Rev. Anim. Biosci.* **2021**, *9*, 355–377. [CrossRef] [PubMed]
4. Listrat, A.; Lebret, B.; Louveau, I.; Astruc, T.; Bonnet, M.; Lefaucheur, L.; Picard, B.; Bugeon, J. How muscle structure and composition influence meat and flesh quality. *Sci. World J.* **2016**, *2016*, 3182746. [CrossRef] [PubMed]
5. Wood, J.D.; Enser, M.; Fisher, A.V.; Nute, G.R.; Sheard, P.R.; Richardson, R.I.; Whittington, F.M.; Hughes, S.I. Fat deposition, fatty acid composition and meat quality: A review. *Meat Sci.* **2008**, *78*, 343–358. [CrossRef] [PubMed]
6. Hausman, G.J.; Dodson, M.V.; Ajuwon, K.; Azain, M.; Barnes, K.M.; Guan, L.L.; Jiang, Z.; Poulos, S.P.; Sainz, R.D.; Smith, S.; et al. Board-invited review: The biology and regulation of preadipocytes and adipocytes in meat animals. *J. Anim. Sci.* **2009**, *87*, 1218–1246. [CrossRef] [PubMed]
7. Vettor, R.; Milan, G.; Franzin, C.; Sanna, M.; De Coppi, P.; Rizzuto, R.; Federspil, G. The origin of intermuscular adipose tissue and its pathophysiological implications. *Am. J. Physiol. Endocrinol. Metab.* **2009**, *297*, E987–E998. [CrossRef]
8. Bakke, S.S.; Moro, C.; Nikolić, N.; Hessvik, N.P.; Badin, P.-M.; Lauvhaug, L.; Fredriksson, K.; Hesselink, M.K.; Boekschoten, M.V.; Kersten, S.; et al. Palmitic acid follows a different metabolic pathway than oleic acid in human skeletal muscle cells; lower lipolysis rate despite an increased level of adipose triglyceride lipase. *Biochim. Biophys. Acta* **2012**, *1821*, 1323–1333. [CrossRef] [PubMed]
9. Xiang, A.; Chu, G.; Zhu, Y.; Ma, G.; Yang, G.; Sun, S. IGFBP5 suppresses oleate-induced intramyocellular lipid deposition and enhances insulin signaling. *J. Cell. Physiol.* **2019**, *234*, 15288–15298. [CrossRef] [PubMed]
10. Mir, B.A.; Albrecht, E.; Ali, A.; Hansson, O.; Maak, S. MicroRNA-100 reduced fetal bovine muscle satellite cell myogenesis and augmented intramuscular lipid deposition by modulating IGF1R. *Cells* **2022**, *11*, 451. [CrossRef] [PubMed]
11. Kivelä, R.; Salmela, I.; Nguyen, Y.H.; Petrova, T.V.; Koistinen, H.A.; Wiener, Z.; Alitalo, K. The transcription factor Prox1 is essential for satellite cell differentiation and muscle fibre-type regulation. *Nat. Commun.* **2016**, *7*, 13124. [CrossRef] [PubMed]
12. Petchey, L.K.; Risebro, C.A.; Vieira, J.M.; Roberts, T.; Bryson, J.B.; Greensmith, L.; Lythgoe, M.F.; Riley, P.R. Loss of Prox1 in striated muscle causes slow to fast skeletal muscle fiber conversion and dilated cardiomyopathy. *Proc. Natl. Acad. Sci. USA* **2014**, *111*, 9515–9520. [CrossRef] [PubMed]
13. Dong, C.; Zhang, X.; Liu, K.; Li, B.; Chao, Z.; Jiang, A.; Li, R.; Li, P.; Liu, H.; Wu, W. Comprehensive analysis of porcine Prox1 gene and its relationship with meat quality traits. *Animals* **2019**, *9*, 744. [CrossRef] [PubMed]
14. Bartel, D.P. MicroRNAs: Target recognition and regulatory functions. *Cell* **2009**, *136*, 215–233. [CrossRef] [PubMed]
15. Sayed, D.; Abdellatif, M. MicroRNAs in development and disease. *Physiol. Rev.* **2011**, *91*, 827–887. [CrossRef] [PubMed]
16. Wang, J.; Yang, L.; Zhang, J.; Gong, J.; Wang, Y.; Zhang, C.; Chen, H.; Fang, X. Effects of microRNAs on skeletal muscle development. *Gene* **2018**, *668*, 107–113. [CrossRef] [PubMed]
17. Singh, G.B.; Cowan, D.B.; Wang, D.Z. Tiny regulators of massive tissue: MicroRNAs in skeletal muscle development, myopathies, and cancer cachexia. *Front. Oncol.* **2020**, *10*, 598964. [CrossRef] [PubMed]
18. van Rooij, E.; Quiat, D.; Johnson, B.A.; Sutherland, L.B.; Qi, X.; Richardson, J.A.; Kelm, R.J.; Olson, E.N. A family of microRNAs encoded by myosin genes governs myosin expression and muscle performance. *Dev. Cell* **2009**, *17*, 662–673. [CrossRef] [PubMed]
19. Wu, J.; He, D.; Yue, B.; Zhang, C.; Fang, X.; Chen, H. miR-101-1 expression pattern in Qinchuan cattle and its role in the regulation of cell differentiation. *Gene* **2017**, *636*, 64–69. [CrossRef] [PubMed]
20. Liu, S.; Xie, S.; Chen, H.; Li, B.; Chen, Z.; Tan, Y.; Yang, J.; Zheng, L.; Xiao, Z.; Zhang, Q.; et al. The functional analysis of transiently upregulated miR-101 suggests a "braking" regulatory mechanism during myogenesis. *Sci. China Life Sci.* **2021**, *64*, 1612–1623. [CrossRef] [PubMed]
21. Kazenwadel, J.; Michael, M.Z.; Harvey, N.L. Prox1 expression is negatively regulated by miR-181 in endothelial cells. *Blood* **2010**, *116*, 2395–2401. [CrossRef] [PubMed]
22. Leslie Pedrioli, D.M.; Karpanen, T.; Dabouras, V.; Jurisic, G.; van de Hoek, G.; Shin, J.W.; Marino, D.; Kälin, R.E.; Leidel, S.; Cinelli, P.; et al. miR-31 functions as a negative regulator of lymphatic vascular lineage-specific differentiation in vitro and vascular development in vivo. *Mol. Cell. Biol.* **2010**, *30*, 3620–3634. [CrossRef] [PubMed]
23. Seo, M.; Choi, J.-S.; Rho, C.R.; Joo, C.-K.; Lee, S.K. MicroRNA miR-466 inhibits lymphangiogenesis by targeting prospero-related homeobox 1 in the alkali burn corneal injury model. *J. Biomed. Sci.* **2015**, *22*, 3. [CrossRef] [PubMed]

24. Nguyen-Vu, T.; Wang, J.; Mesmar, F.; Mukhopadhyay, S.; Saxena, A.; McCollum, C.W.; Gustafsson, J.; Bondesson, M.; Williams, C. Estrogen receptor beta reduces colon cancer metastasis through a novel miR-205-PROX1 mechanism. *Oncotarget* **2016**, *7*, 42159–42171. [CrossRef] [PubMed]
25. Zhang, B.; Ji, S.; Ma, F.; Ma, Q.; Lu, X.; Chen, X. miR-489 acts as a tumor suppressor in human gastric cancer by targeting PROX1. *Am. J. Cancer Res.* **2016**, *6*, 2021–2030. [PubMed]
26. Mir, B.A.; Reyer, H.; Komolka, K.; Ponsuksili, S.; Kühn, C.; Maak, S. Differentially expressed miRNA-gene targets related to intramuscular fat in Musculus longissimus dorsi of Charolais × Holstein F2-crossbred bulls. *Genes* **2020**, *11*, 700. [CrossRef] [PubMed]
27. Komolka, K.; Ponsuksili, S.; Albrecht, E.; Kühn, C.; Wimmers, K.; Maak, S. Gene expression profile of Musculus longissimus dorsi in bulls of a Charolais × Holstein F2-cross with divergent intramuscular fat content. *Genom. Data* **2016**, *7*, 131–133. [CrossRef] [PubMed]
28. Agarwal, V.; Bell, G.W.; Nam, J.-W.; Bartel, D.P. Predicting effective microRNA target sites in mammalian mRNAs. *eLife* **2015**, *4*, e05005. [CrossRef]
29. Will, K.; Schering, L.; Albrecht, E.; Kalbe, C.; Maak, S. Differentiation of bovine satellite cell-derived myoblasts under different culture conditions. *Vitr. Cell. Dev. Biol. Anim.* **2015**, *51*, 885–889. [CrossRef] [PubMed]
30. Hellemans, J.; Mortier, G.; De Paepe, A.; Speleman, F.; Vandesompele, J. qBase relative quantification framework and software for management and automated analysis of real-time quantitative PCR data. *Genome Biol.* **2007**, *8*, R19. [CrossRef] [PubMed]
31. Mir, B.A.; Islam, R.; Kalanon, M.; Russell, A.P.; Foletta, V.C. MicroRNA suppression of stress-responsive NDRG2 during dexamethasone treatment in skeletal muscle cells. *BMC Mol. Cell Biol.* **2019**, *20*, 12. [CrossRef] [PubMed]
32. Schering, L.; Albrecht, E.; Komolka, K.; Kühn, C.; Maak, S. Increased expression of thyroid hormone responsive protein (THRSP) is the result but not the cause of higher intramuscular fat content in cattle. *Int. J. Biol. Sci.* **2017**, *13*, 532–544. [CrossRef] [PubMed]
33. Dahl, N.; Albrecht, E.; Dannenberger, D.; Uken, K.L.; Hammon, H.M.; Maak, S. Consequences of maternal essential fatty acid and conjugated linoleic acid supplementation on the development of calf muscle and adipose tissue. *Animals* **2020**, *10*, 1598. [CrossRef] [PubMed]
34. Gumucio, J.P.; Qasawa, A.H.; Ferrara, P.J.; Malik, A.N.; Funai, K.; Mcdonagh, B.; Mendias, C.L. Reduced mitochondrial lipid oxidation leads to fat accumulation in myosteatosis. *FASEB J.* **2019**, *33*, 7863–7881. [CrossRef] [PubMed]
35. Ahn, B.; Soundarapandian, M.M.; Sessions, H.; Peddibhotla, S.; Roth, G.P.; Li, J.-L.; Sugarman, E.; Koo, A.; Malany, S.; Wang, M.; et al. MondoA coordinately regulates skeletal myocyte lipid homeostasis and insulin signaling. *J. Clin. Investig.* **2016**, *126*, 3567–3579. [CrossRef] [PubMed]

Disclaimer/Publisher's Note: The statements, opinions and data contained in all publications are solely those of the individual author(s) and contributor(s) and not of MDPI and/or the editor(s). MDPI and/or the editor(s) disclaim responsibility for any injury to people or property resulting from any ideas, methods, instructions or products referred to in the content.